Expanded View Figures

Figure EV1. Pore-forming assay using BakΔTM and BclxLΔTM bound to Ni^{2+}-caged lipids in liposomes.

A, B The data are averaged for the time frame of 9,000–10,000 s and the standard deviation calculated from three measurements, respectively. (A) Influence of Ni^{2+}-caged lipids on BakΔTM activity. Liposomes were formed with OMM-like lipids and subjected to 50 nM BakΔTM ± 20 nM cBid. (B) Influence of the indicated lipid compositions on BakΔTM autoactivity.

C Influence of cBid (300 nM) and BclxLΔTM (300 nM) on BakΔTM (600 nM), when autoactive.

D Comparison of the effect of BclxLΔTM on 600 nM BakΔTM pore formation with and without a His-tag. The inhibitory activity of BclxL is highly dependent on its stable membrane association.

E Far-UV-CD spectra of BakΔTM ± *E. coli* polar liposomes and the Puma-BH3 peptide as indicated.

F CD-detected thermal melting experiments of BakΔTM (black) with liposomes (red) and Puma-BH3 (blue).

G Percentile dye release is shown after 420 s for 600 nM BakΔTM ± 300 nM of an activator. The data are averaged for the time frame of 9,000–10,000 s and the standard deviation calculated from three technical replicates, respectively. Both cBid and Puma-BH3 lead to enhanced liposome permeabilization.

Data information: (C–G) Liposomes were formed using *E. coli* polar lipids.

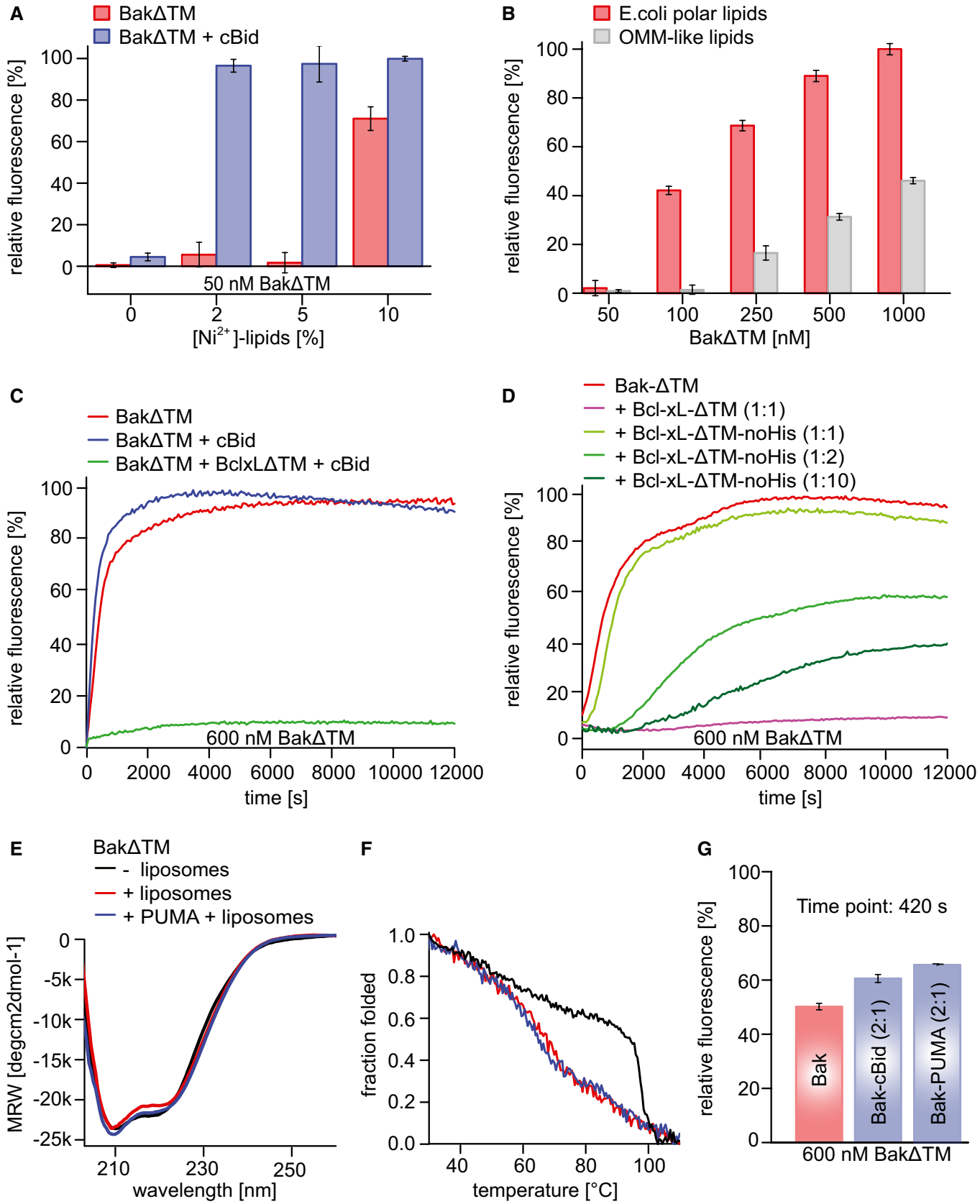

Figure EV1.

Figure EV2. NMR structural characterization of the Bak soluble domain and the TMH.

A NMR secondary chemical shifts of BakΔTM are in agreement with the α-helical secondary structure content as present in a crystal structure (2IMS.pdb (Moldoveanu *et al*, 2006)) indicated at the top.

B Correlation between the experimental and back-calculated RDCs for the NMR-refined BakΔTM structure.

C Comparison of the refined BakΔTM structure containing the full N-terminus with the published crystal structure (2IMS.pdb (Moldoveanu *et al*, 2006)), which was used as an initial structure for the refinement.

D Comparison of the sequence and structure of the Bak- and BclxL-TMH in nanodiscs. The high similarity is shown by color coding the amino acids according to their polarity (red: apolar, green: polar, blue: basic). Identical amino acids are highlighted in the sequence in gray.

E SEC profiles of Bak-TMH in nanodiscs after cleaving off the GB1 tag color-coded according to the table on the right. The area under the curve was used to calculate the ratio of TMH/nanodisc. The table shows the applied assembly conditions as well as the expected and calculated amount of TMH/nanodisc. For a dimeric protein like the glycophorin A (GlyA) TMH, the expected and calculated ratios vary, which is not the case for the Bak-TMH.

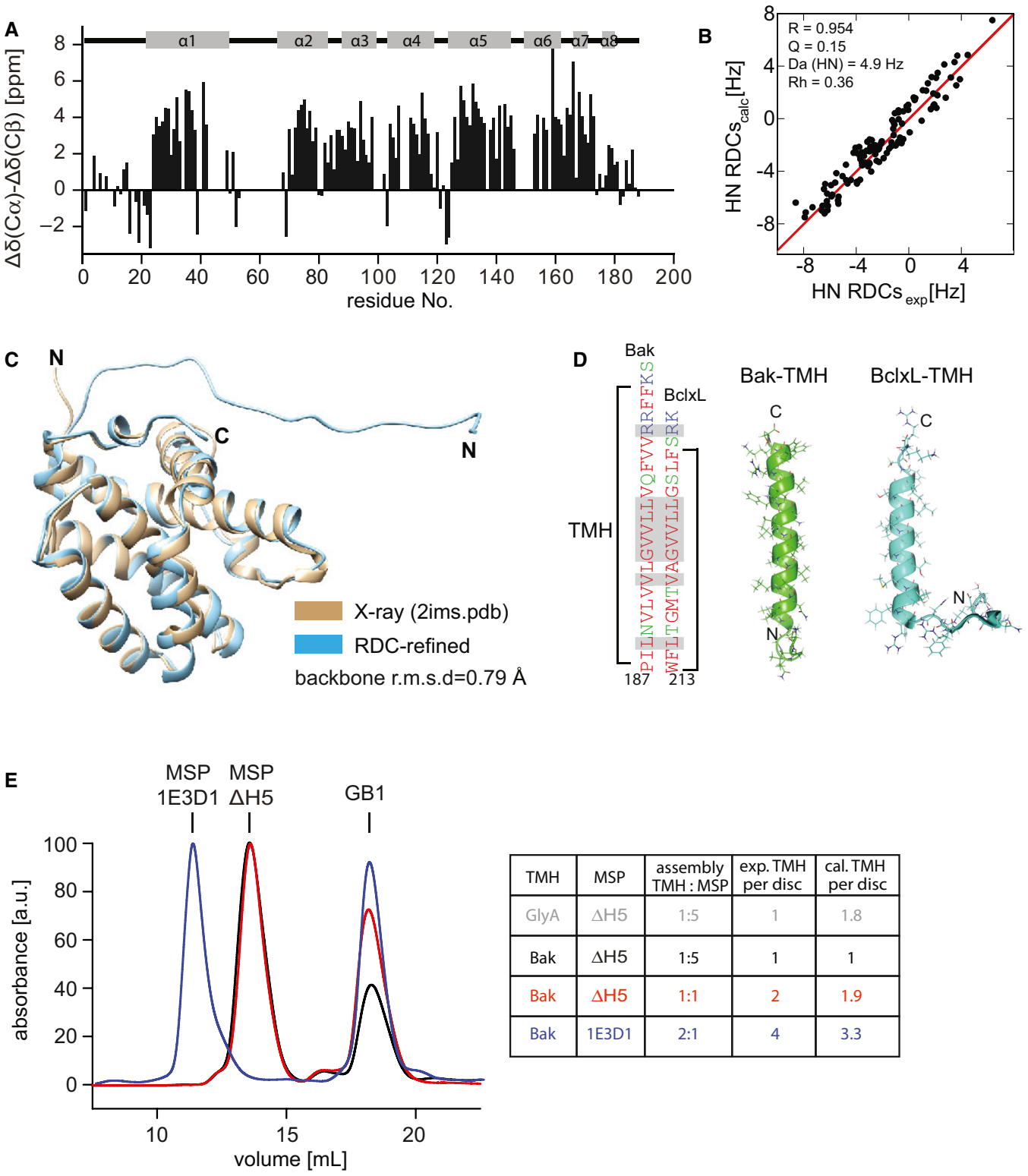

TMH	MSP	assembly TMH : MSP	exp. TMH per disc	cal. TMH per disc
GlyA	ΔH5	1:5	1	1.8
Bak	ΔH5	1:5	1	1
Bak	ΔH5	1:1	2	1.9
Bak	1E3D1	2:1	4	3.3

Figure EV2.

Figure EV3. Biophysical characterization of soluble BakΔTM and BclxLΔTM.

A 2D-[^{15}N, ^{1}H]-HSQC spectra of BakΔTM (left) and BclxLΔTM (right) using a protonated (black) or deuterated (red) sample.
B DLS experiments of BakΔTM (left) and BclxLΔTM (right) upon incubation at different temperatures and varying times. The tables on the right state the hydrodynamic diameter in [nm], which is calculated from the measured hydrodynamic radii.
C Tryptophan fluorescence emission spectra of BakΔTM at different GuHCl concentrations upon excitation at 280 nm.
D Fluorescence emission spectra of SYPRO Orange binding to BakΔTM at different GuHCl concentrations.
E 2D-[^{15}N, ^{1}H]-HSQC spectra of BakΔTM in the absence (black) and presence of 1.5 M GuHCl (red) and 2.5 M GuHCl (magenta).

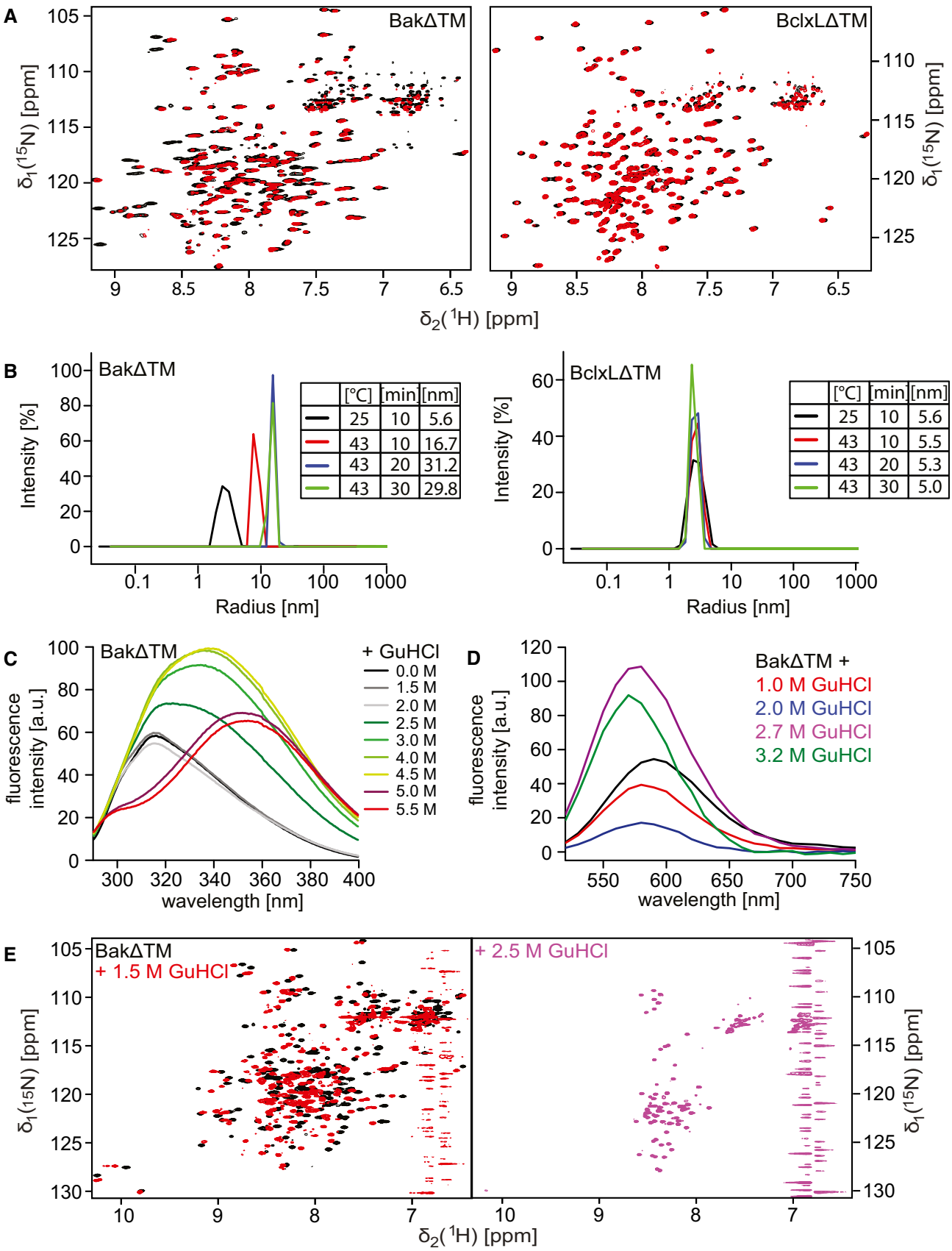

Figure EV3.

Figure EV4. Characterization of BakΔTM stability and pore-forming activity in nanodiscs and liposomes.

A Far-UV-CD thermal melting data of BakΔTM bound to lipid nanodiscs. The melting point at 68.4°C corresponds to BakΔTM, while the later unfolding event at 79.7°C shows the melting of the MSP forming the nanodisc.

B SDS–PAGE of Cu/phen crosslinking of BakΔTM bound to ΔH5 nanodiscs ± Bid-BH3 peptide.

C Size exclusion chromatogram of BakΔTM bound to nanodiscs after activation by Bid-BH3. Inset: SDS–PAGE shows that activated BakΔTM elutes before the main nanodisc peak. The MSP band is very faint due to increased destaining which is sometimes seen for MSP.

D Pore-forming assay with 600 nM BakΔTM in liposomes of 30 nm size.

E Comparison of the deuterium uptake of the active Bak species in liposomes (black) and ΔH5 nanodiscs (blue). The HDX-MS detected deuterium uptake is compared after 10 s at the top and 2 h at the bottom.

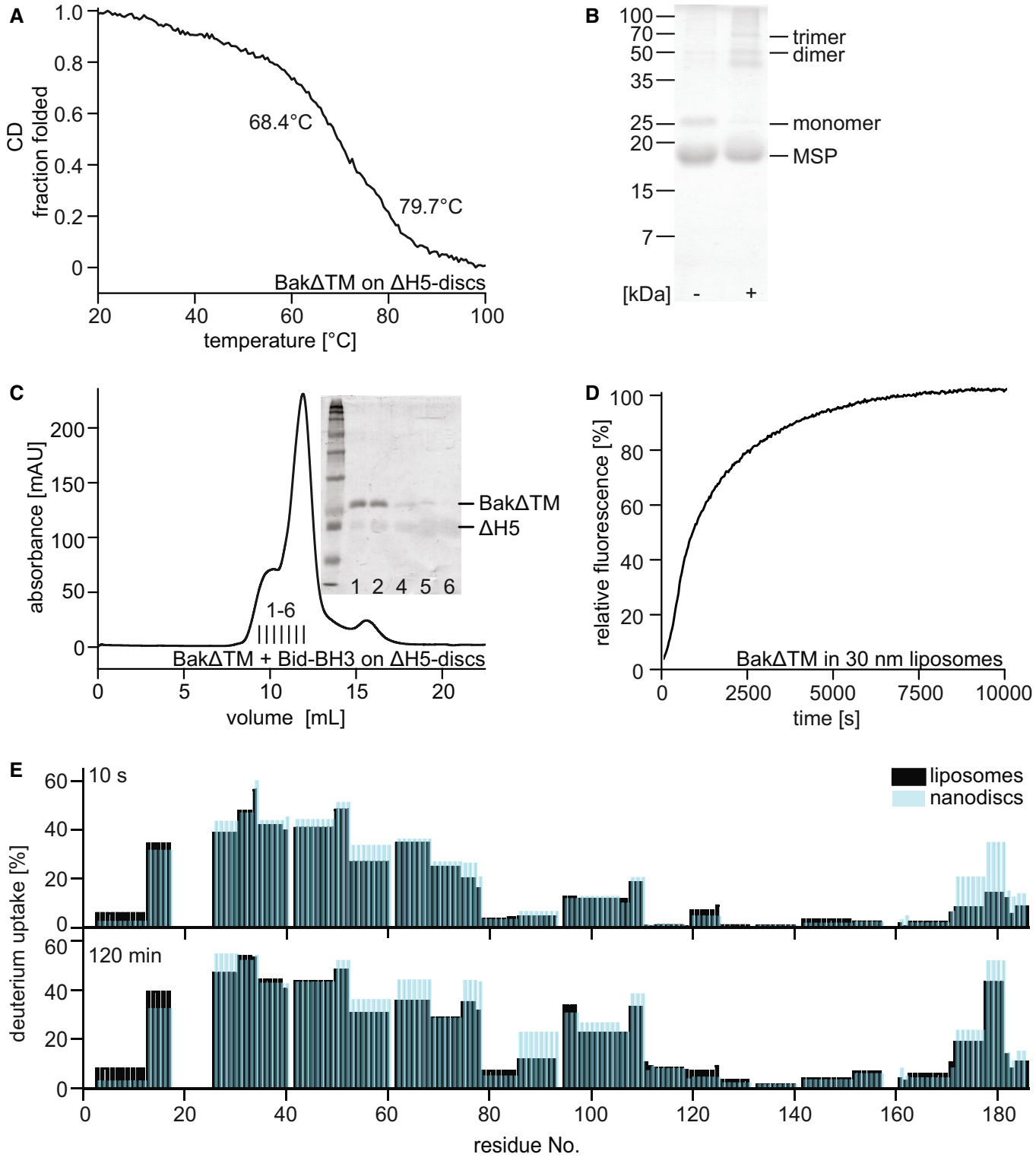

Figure EV4.

Figure EV5. HDX-MS data of BakΔTM.

A HDX peptide coverage maps of the different BakΔTM samples. BakΔTM: Total coverage was 100% with 126 peptides and a redundancy of 6.96. BakΔTM + ΔH5 nanodiscs (inactive): Total coverage was 99% with 83 peptides and a redundancy of 4.47. BakΔTM + ΔH5 nanodiscs + Bid-BH3 (active): Total coverage was 97% with 76 peptides and a redundancy of 4.25.

B HDX graphs of three peptides, located in different helices as indicated, displaying the relative deuterium uptake during the reaction time. Two biological replicates were measured for each state. (ND = ΔH5 nanodiscs).

C HDX-MS experiments of unbound BakΔTM and BakΔTM bound to Ni-nanodiscs in the inactive state and after activation with the Bid-derived BH3 peptide. HDX was mapped to the BakΔTM structure and colored according to the measured exchange rates after the incubation times indicated. Blue colors correspond to a lower (less accessible) and red colors to a higher (more accessible) fractional uptake of deuterium.

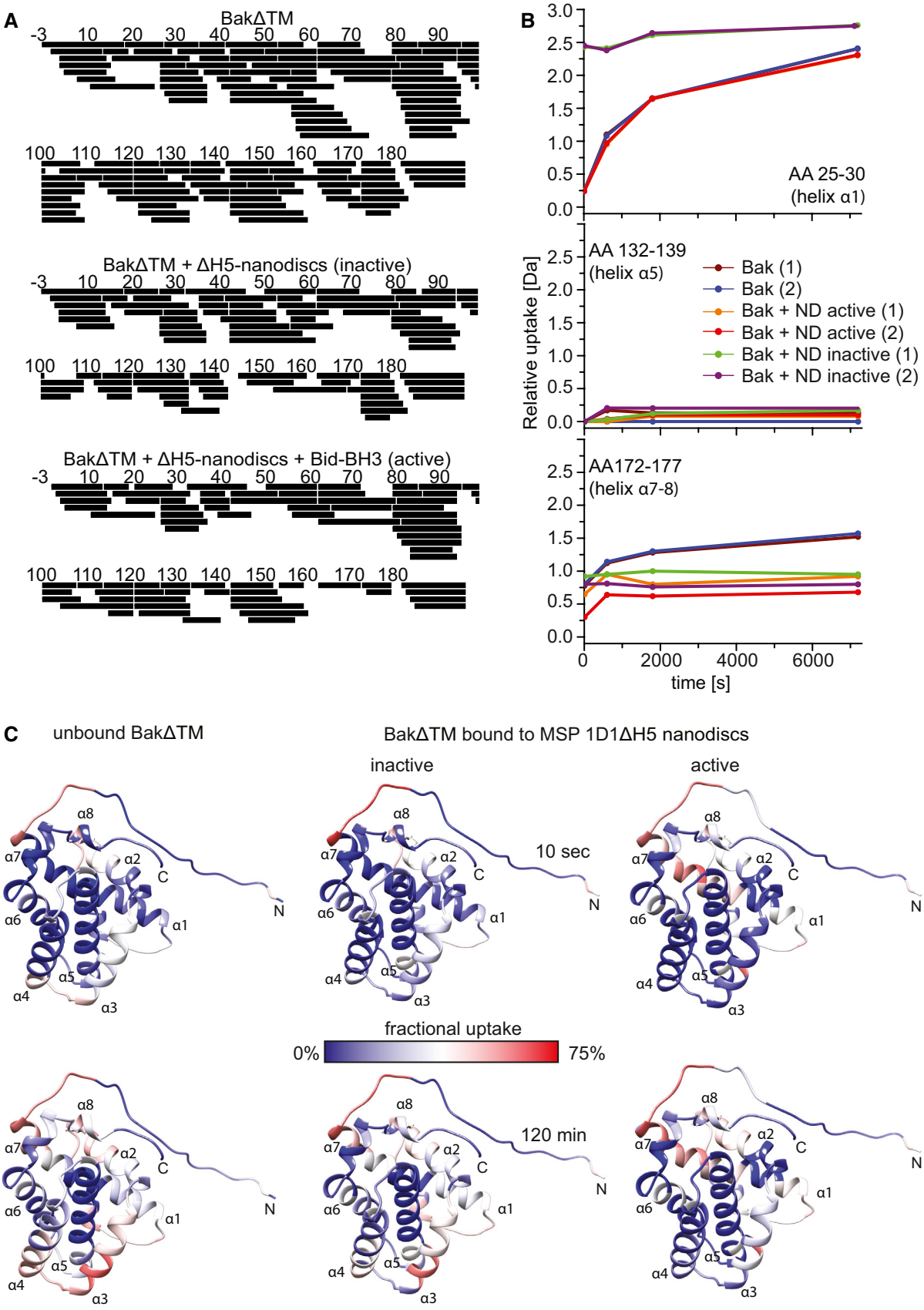

Figure EV5.